Supporting Information

Activating Multimetallic Phosphides *via* Plasma-Induced Phosphorus Vacancies for Efficient Water Electrolysis

Yang Yang,[a] Zhi-Yuan Jiang[a], Peng-Fei Guo[a,c], Min-Huan Zhang[a], Jian-Hua Meng[a], Ran Jin[b], Ke-Xiang Wang[a], Ran Ma,*[a] and Xun Cui*[b]*

[a]Key Laboratory of Chemical Additives for China National Light Industry, College of Chemistry and Chemical Engineering, Shaanxi University of Science and Technology, Xi'an, 710021, China.

[b]State Key Laboratory of New Textile Materials and Advanced Processing Technologies, Wuhan Textile University, Wuhan, 430200, China.

[c]Key Laboratory of Aerospace Chemistry, Inner Mongolia Institute of Synthetic Chemical Research, Hohhot, 010000, China.

Corresponding Authors

*E-mail: yyang399@sust.edu.cn (Yang Yang)

maran@sust.edu.cn (Ran Ma)

xcui@wtu.edu.cn (Xun Cui)

Contents

1. Experimental Section

1.1. Chemicals and Materials

All chemical reagents were purchased from commercial suppliers and did not require further purification before use. Nickel (II) nitrate hexahydrate ($Ni(NO_3)_2 \cdot 6H_2O$, Macklin, AR, 98%), iron (II) chloride tetrahydrate ($FeCl_2 \cdot 4H_2O$, 99.5%, CAS No.13478-10-9, Macklin), tungsten chloride (WCl_6, 99%, CAS No.13283-01-7, Macklin), ammonium fluoride (NH_4F; 98%, CAS No. 12125-01-8, Aladdin), urea (CH_4N_2O; 99%, CAS No.57-13-6, Aladdin), potassium hydroxide (KOH; 90%, CAS No. 1310-58-3, Macklin), platinum carbon (Pt/C, 20 wt%,Aldrich,), iridium dioxide (IrO_2, 99.9%, CAS No.12030-49-8). All ultrapure water (18.2 MΩ cm) in this work was obtained using an Ulupure UPR-III-10T (Sichuan YOUPU Ultrapure Technology Corporation) system. Nickel foam (thickness ~3 mm) was purchased from Kunshan Lvchuang Electronic Technology Co., Ltd.

1.2. Materials Synthesis

1.2.1. Treatment of nickel foam (NF)

Nickel foam (1 cm × 4 cm) was first treated for 5 min on the front and back sides under a high-purity Ar (99.999%) atmosphere at 100 W power *via* a plasma-enhanced chemical vapor deposition (PECVD, OTF-1200X-80-II-4CV-PE-SL, Hefei Kejing Materials Technology Corporation) system. Then, the resulting NF was dipped into 1

M HCl solution, acetone, ethanol, and ultrapure water in turn, cleaned with an ultrasonic washer for 10 min, and finally dried with N_2.

1.2.2. Preparation of the NiFeW LDH/NF catalyst

All LDH catalysts in this chapter were produced using a one-step solvothermal method, which is as follows: First, 118.9 mg WCl_6 was completely dissolved in 10 mL of ethylene glycol solution, which was heated to 50 °C to achieve the dissolution effect; then, 348.9 mg $Ni(NO_3)_2 \cdot 6H_2O$, 59.6 mg $FeCl_2 \cdot 4H_2O$ and 333.0 mg NH_4F were dissolved in 30 mL of ultrapure water. The precursor solution was produced by completely integrating the foregoing two solutions, adding 540.5 mg of urea, and dissolving the mixture until it was clear and transparent. Finally, the treated NF (1 × 4 cm) was reacted with the precursor solution at 120 °C for 6 hours. After cooling down to room temperature, it was scrubbed with water and ethanol, blown dry with nitrogen, and stored.

The preparation of NiW LDH/NF was basically the same as that of NiFeW LDH/NF, except that $FeCl_2 \cdot 4H_2O$ was not added and the amount of WCl_6 was doubled.

1.2.3. Preparation of the NiFeWP/NF catalyst

The previously mentioned NiFeW LDH/NF was placed in a plasma-enhanced chemical vapor deposition furnace, heated to 300 °C at a rate of 5 °C min^{-1} under vacuum conditions, and held at this temperature for 10 minutes. Then, a 10% PH_3/Ar mixture was introduced, and the furnace pressure was kept at around 75 Pa. The reaction was completed in 10 minutes while the radio frequency power supply was set at 150 W.

After being brought down to room temperature, the catalyst was taken out from the plasma chemical vapor deposition furnace.

1.2.4. Preparation of the NiFeWP(V_P)/NF catalyst

The preparation process of NiFeWP(Vp)/NF was exactly the same as that of NiFeWP/NF described above, with the exception that after completing the phosphorylation conversion in a 10% PH_3/Ar mixture, the 10% PH_3/Ar mixture was changed to high-purity N_2 gas, and the reaction was continued for 10 minutes under the same conditions (keeping the pressure and power unchanged) before the process was stopped, and was taken out after cooling to room temperature.

NiWP(V_P)/NF was prepared under the same experimental conditions.

1.3. Materials Characterization

The crystal structure of the catalysts was determined using a Powder X-Ray Diffractometer (XRD) type D8 ADVANCE from Bruker in Germany. The radiation source was Cu-Kα (λ = 0.154 nm), the operating voltage was 40 kV, and the operating current was 40 mA. Data was collected at a scan rate of 5 min^{-1} through a 2θ range of 5-70. The surface elemental valence and composition of the catalyst materials were identified using X-ray Photoelectron Spectroscopy (XPS) using an ESCALAB 250xi from Thermo Fisher, USA. Test parameters: The radiation source was Al-Kα (*hv*=1486.6 eV), with an accelerating voltage of 16 kV and an accelerating current of 14.9 mA. And the charge calibration was done at C 1s=284.8 eV. The morphology of

the catalyst materials was analyzed using a Sigma 300 Field Emission Scanning Electron Microscope (FESEM) manufactured by Zeiss, Germany, at an accelerating voltage of 3 kV. The atomic composition of the catalyst material surface was determined by an Xplore-type Energy Dispersive Spectroscopy (EDS) equipped with Oxford, UK, at an accelerating voltage of 15 kV and the elemental distribution was determined by photographing the energy spectrum mapping. A Talos F200X scanning transmission electron microscope (STEM) manufactured by Thermo Fisher, USA, was used to collect HRTEM images and surface scanning images of the catalyst materials at an operating voltage of 200 kV to further characterize the catalyst materials. The microstructures of the catalyst materials were further characterized by their microstructures, crystal structure types, atomic arrangement, and exposed crystal surfaces. An Electron Paramagnetic Resonance (EPR) spectrometer (EMX Plus-6/1) from Bruker, Germany, was used to detect the presence of vacancies in the catalyst material. Test parameters: Scanning width of 6000 G, operating frequency of 9.8 GHz, and 2,2,6,6-tetramethylpiperidine oxide (TEMPO) as vacancy capture agent. The elemental composition of the catalyst materials was analyzed using an inductively coupled plasma mass spectrometer (ICP-MS, Agilent 7800, USA). In situ Raman spectra were collected using a RENISHAW in *Via* Raman Microscope equipped with a confocal optical system. The measurements were conducted in 0.1 M KOH using a standard three-electrode configuration, with a platinum wire as the counter electrode and an Ag/AgCl electrode as the reference electrode. The Raman spectra were recorded in the wavenumber range of 200-1200 cm^{-1}.

1.4. Electrochemical Characterization

All electrochemical tests were carried out under a conventional three-electrode system using a Chenhua electrochemical workstation CHI 760E in a 1.0 M KOH solution.

For measurements of the hydrogen evolution reaction, carbon rods and Hg/HgO electrodes were used as counter electrodes and reference electrodes, respectively. Before performing the measurements, high-purity hydrogen (99.999%) was passed into the system for 30 min and maintained throughout the test to ensure that the 1.0 M KOH electrolyte was always saturated with hydrogen. LSV polarization curves were measured at a scan rate of 5 mV s^{-1}. CV testing were conducted in the non-Faraday zone (-0.7 to -0.8 V *vs.* Hg/HgO) at various scan rates (20, 40, 60, 80, 100, and 120 mV s^{-1}). C_{dl} was calculated from the linear dependency of the difference in current density Δj ($\Delta j=(j_{anode}-j_{cathode})/2$) at -0.75 V vs scan rate. Electrochemical impedance spectra (EIS) were obtained from 1 kHz to 130 kHz at a voltage of -1.05 V (*vs.* Hg/HgO). Catalyst durability experiments were performed using chronopotentiometry at a fixed current density (10 mA cm^{-2}).

To measure the oxygen evolution reaction, a platinum wire and a Hg/HgO electrode were employed as counter and reference electrodes, respectively. High-purity oxygen (99.999%) was injected into the system for 30 minutes and maintained throughout the test to ensure that the 1.0 M KOH electrolyte was always oxygenated. The LSV polarization curves were recorded at a scan rate of 5 mV s^{-1} throughout a voltage range of 1.1-1.7 V (vs. Hg/HgO). CV testing were conducted in the non-

Faraday zone (0.2 to 0.3 V *vs.* Hg/HgO) at various scan rates (20, 40, 60, 80, 100, and 120 mV s^{-1}). electrochemical impedance spectra (EIS) were obtained from 350 Hz to 150 kHz at a voltage of 0.55 V (*vs.* Hg/HgO). Catalyst durability experiments were performed using chronopotentiometry at a fixed current density (10 mA cm^{-2}). By applying the Nernst equation, all of the potentials mentioned above involving Hg/HgO were transformed into reversible hydrogen electrodes. All polarization curves were corrected by 95% iR to compensate for the loss of solution resistance.

$$E_{RHE}=E_{Hg/HgO}+0.059pH+0.098$$

The Tafel slope, which describes the relationship between overpotential (η) and current density (j), is used to characterize the electrode reaction kinetics of catalysts. It is calculated by the following equation:

$$\eta = a + b\cdot\log|j|$$

The double-layer capacitance (C_{dl}) of the catalyst was measured by cyclic voltammetry. The electrochemical stability of the catalyst was evaluated by chronopotentiometry, which involves obtaining the potential-time (E-t) curve at a specific current density.

The catalysts were directly grown on Ni foam substrates with a geometric area of 1 × 4 cm^2. The mass loading was determined by weighing the Ni foam before and after the synthesis using an analytical balance. For each sample, three independent measurements were performed and the average value was reported. The average catalyst loading of NiFeWP(V_P) was approximately 2.7 mg cm^{-2}, corresponding to mass increases of 11.2, 8.7, and 12.6 mg for the three electrodes. For NiWP(V_P), the average

catalyst loading was approximately 2.95 mg cm^{-2}, with mass increases of 13.1, 11.6, and 10.7 mg, respectively. All current densities reported in this work were normalized to the geometric area of the electrode.

2. Additional Data and Figures

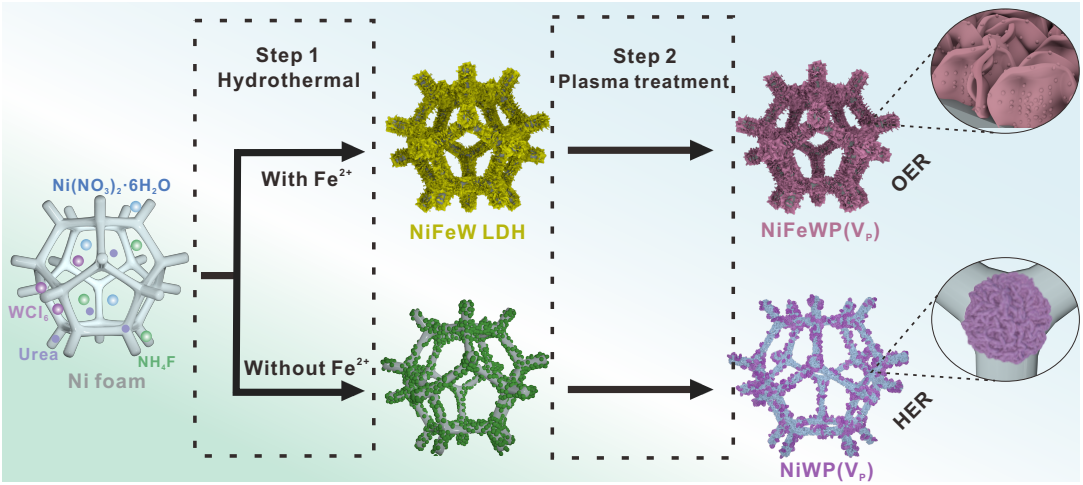

Fig. S1. Schematic of catalyst synthesis.

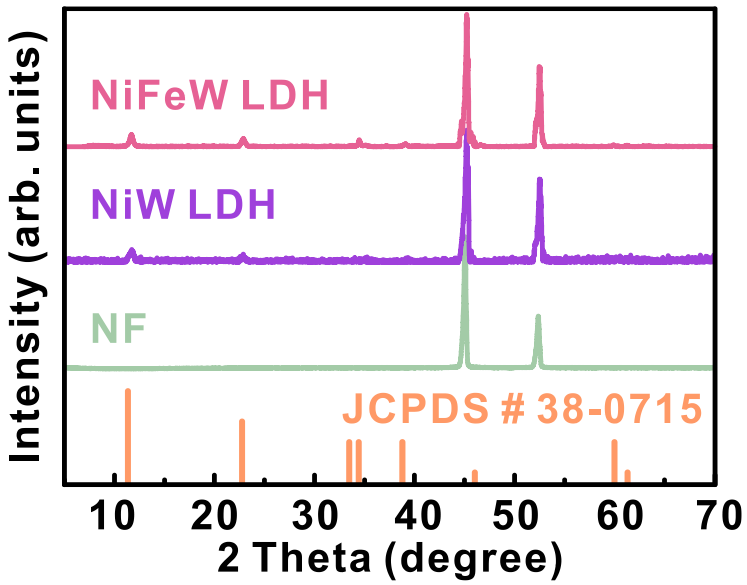

Fig. S2. XRD patterns of NiFeW LDH and NiW LDH.

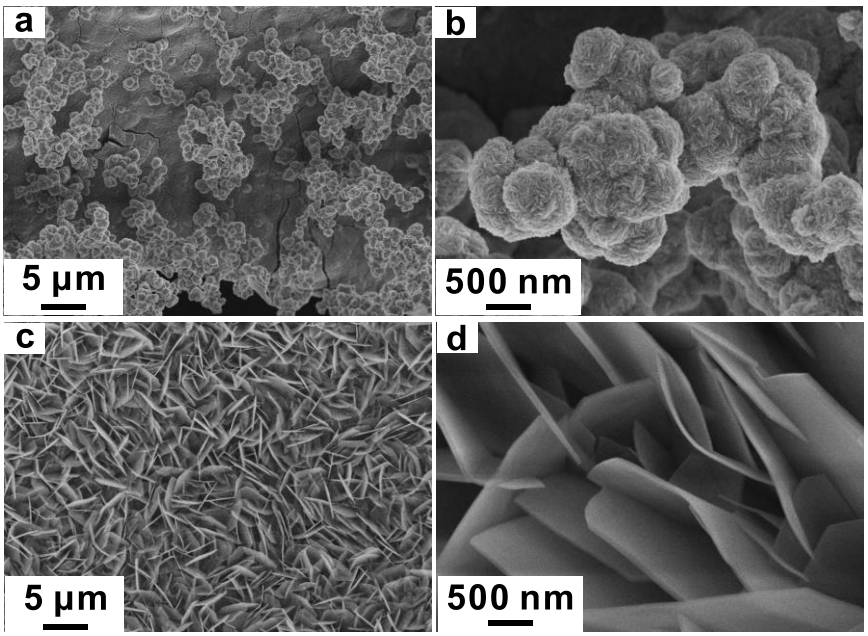

Fig. S3. SEM images of (a, b) NiW LDH, and (c, d) NiFeW LDH.

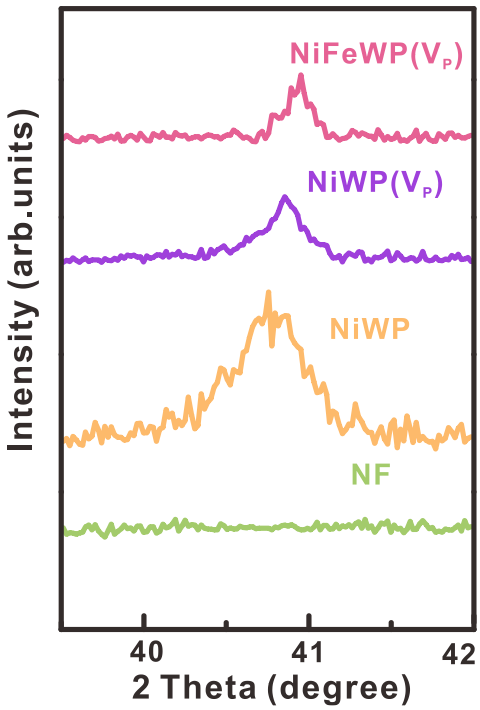

Fig. S4. Enlarged XRD diffraction region of the samples in the 2θ range of 40–42°.

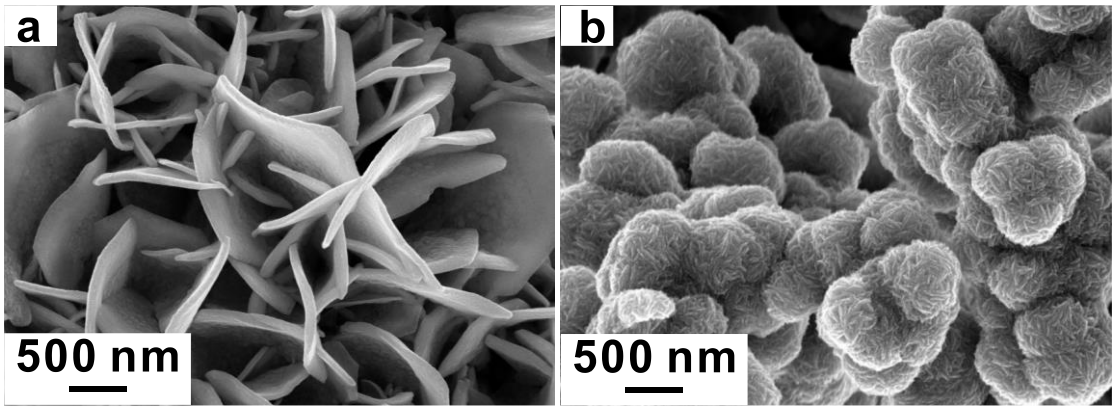

Fig. S5. (a) SEM images of NiFeWP(V_P); (b) SEM images of NiWP(V_P).

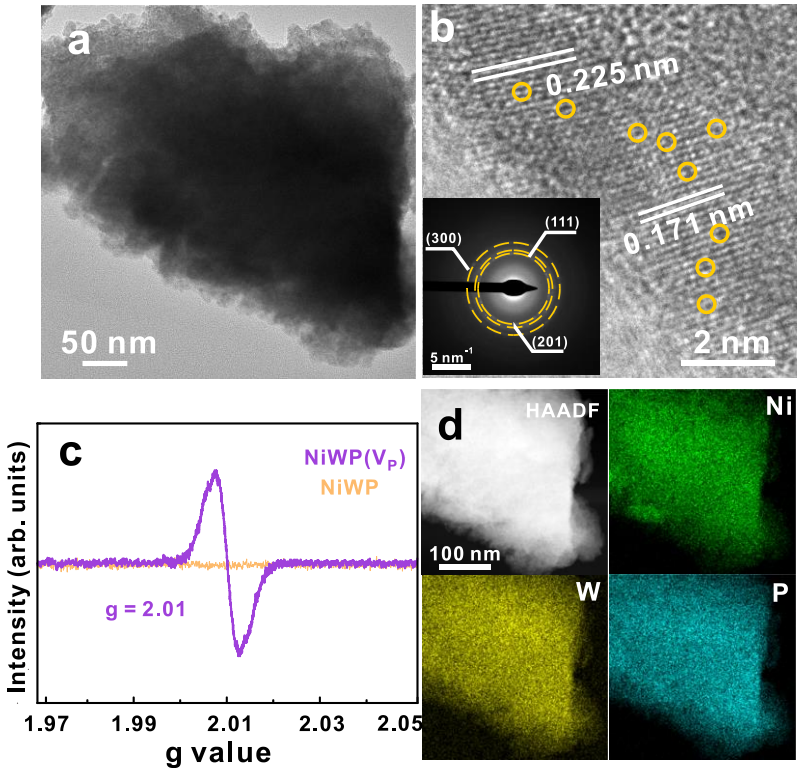

Fig. S6. (a) TEM image of NiWP(V_P); (b) HRTEM image of NiWP(V_P) (Circles mark lattice discontinuities) with an inset SAED patterns; (c) EPR spectrum of NiWP(V_P); (d) HAADF-STEM image and the corresponding EDS elemental mappings.

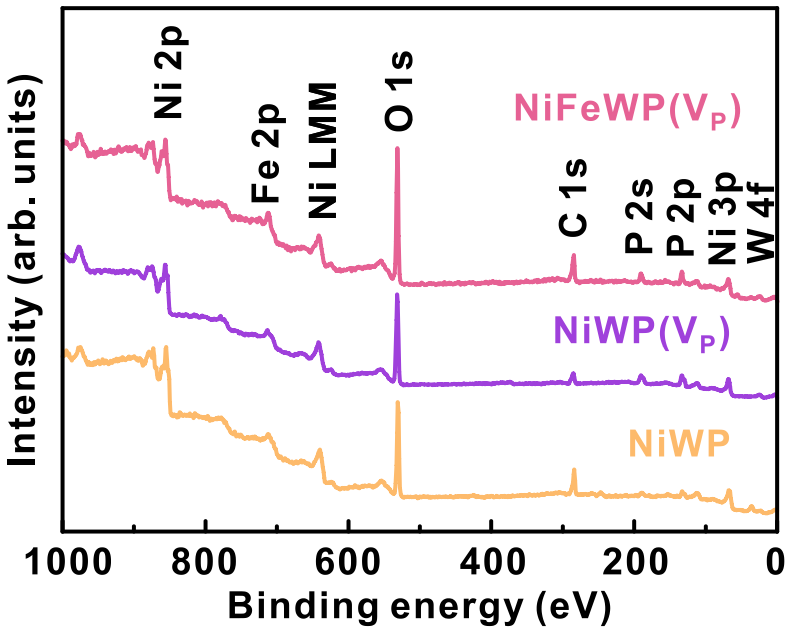

Fig. S7. XPS full spectrum of NiFeWP(V_P), NiWP(V_P) and NiWP.

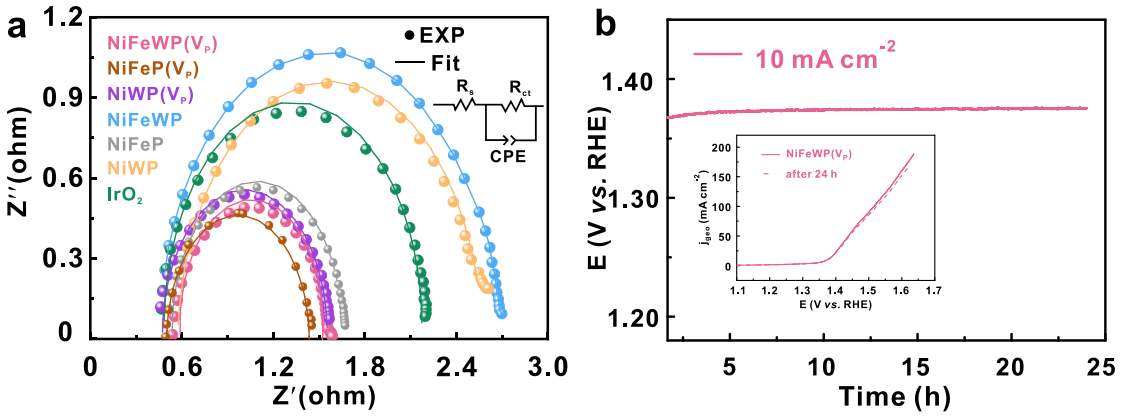

Fig. S8. (a) EIS values of NiFeWP(V_P), NiFeWP, NiFeP(V_P), NiFeP, NiWP(V_P), NiWP and IrO_2 electrodes in 1 M KOH. (b) chronopotential curves for 10 mA cm^{-2}, inset shows LSV before and after OER stability tests.

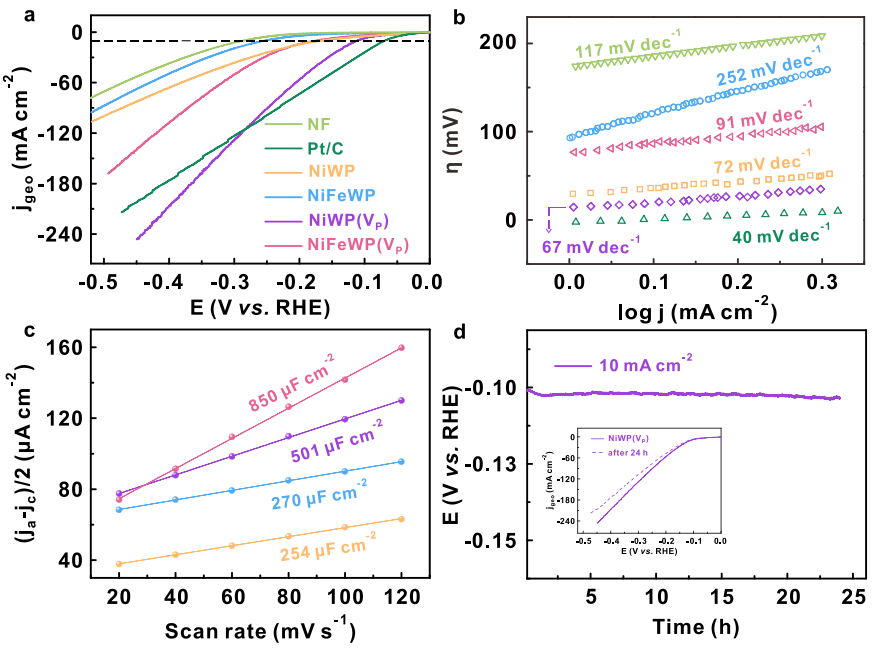

Fig. S9. (a) HER LSV curves, (b) Tafel plots and (c) C_{dl} values of NiFeWP(V_P), NiWP(V_P), NiFeWP, NiWP, NF and IrO_2 electrodes in 1 M KOH; (h) chronopotential curves for 10 mA cm^{-2}, inset shows LSV before and after HER stability tests.

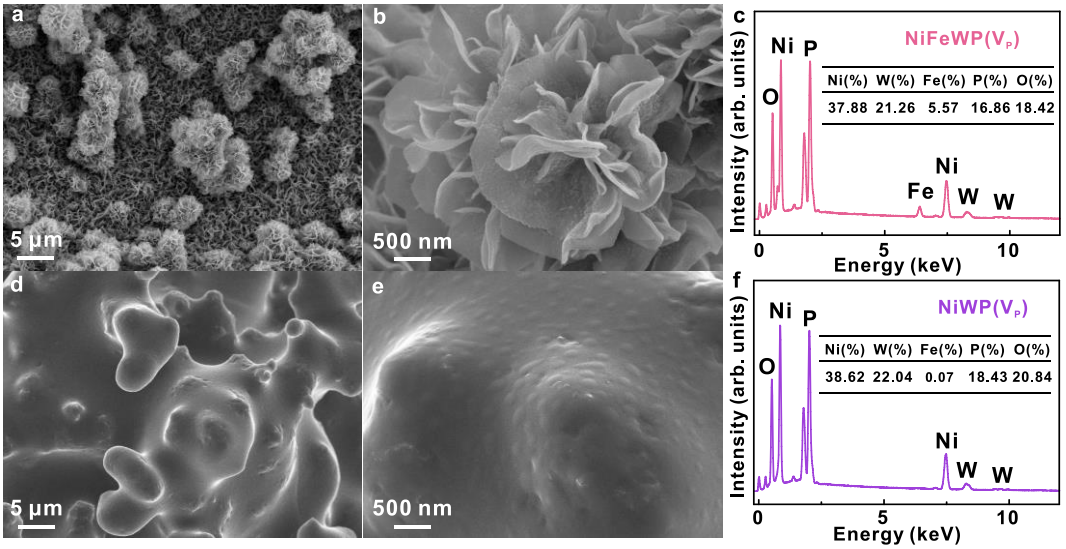

Fig. S10. Characterization of materials after OWS stability testing. (a) and (b) SEM image of NiFeWP(V_P); (c) EDS spectra of NiFeWP(V_P); (d) and (e) SEM image of NiWP(V_P); (f) EDS spectra of NiWP(V_P).

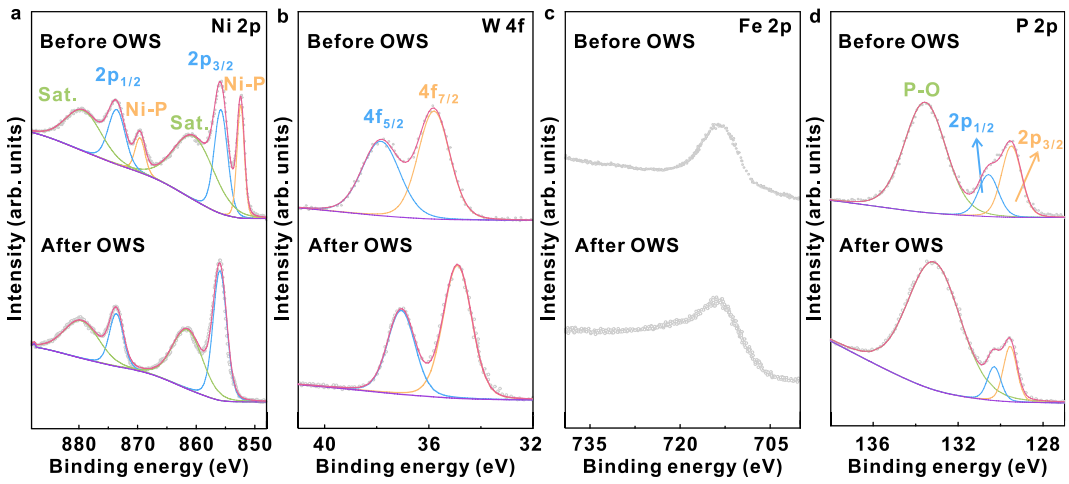

Fig. S11. High-resolution XPS spectra of NiWP(V_P) before and after OWS stability tests. (a)Ni 2p; (b)W 4f; (c)Fe 2p; (d)P 2p.

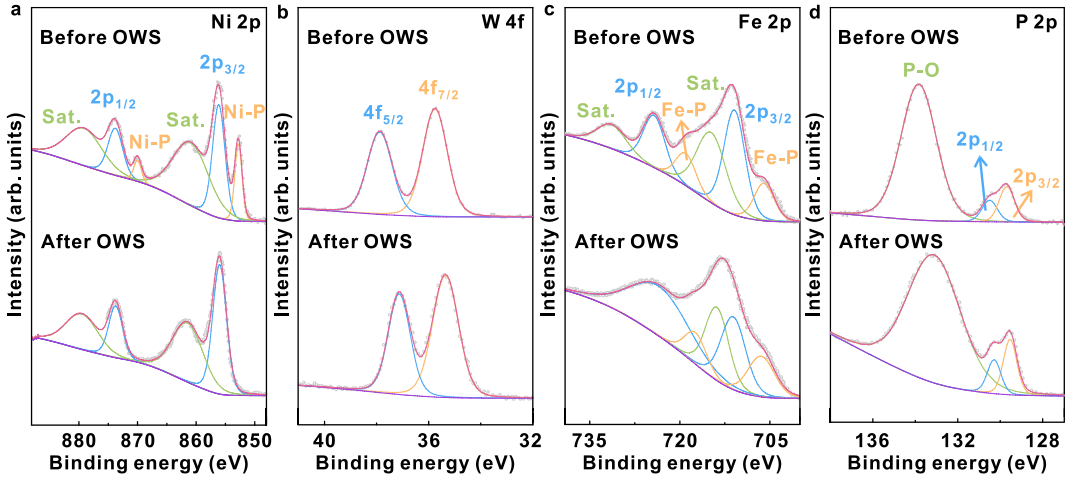

Fig. S12. High-resolution XPS spectra of NiFeWP(V_P) before and after OWS stability tests. (a)Ni 2p; (b)W 4f; (c)Fe 2p; (d)P 2p.

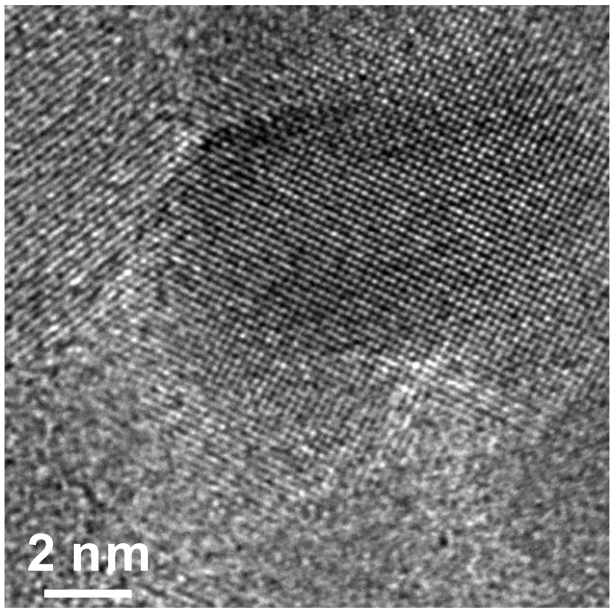

Fig. S13. Original HRTEM image of NiFeWP(V_P) without any annotations.

Table S1. Elemental atomic percentage contents of different catalysts determined by ICP-MS.

Catalysts	Elements/%		
	Ni	Fe	W
NiFeWP(V_P)	86.05	0.68	1.39
NiWP(V_P)	89.89	\	4.35

The elemental compositions of the catalysts were quantitatively determined by inductively coupled plasma mass spectrometry (ICP-MS, Agilent 7800). Prior to analysis, the samples were digested as a whole together with the Ni foam skeleton, and the total digested mass included both the deposited catalyst layer and the Ni foam substrate. The digested solutions were then diluted to a fixed volume before measurement.

The ICP-MS measurements were performed under the following conditions: RF power of 1500 W, pump rate of 30 r/min, nebulizer gas flow rate of 0.78 L/min, auxiliary gas flow rate of 1.2 L/min, and a sample flush time of 15 s.

The elemental concentrations of Ni, Fe, and W in the digested solutions were obtained directly from the ICP-MS instrument. The elemental content (C_x, mg kg^{-1}) was calculated according to the following equation:

$C_x = C_0$ (μg L^{-1}) × V_0 (mL) × 10^{-3} / m_0 (g) × 10^3

Where C_0 is the measured elemental concentration in the solution, V_0 is the final volume of the digested solution, and m_0 is the total mass of the digested sample. The weight percentage (W%) of

each element was further calculated based on the corresponding elemental contents. The ICP-MS results are mainly used to evaluate the incorporation of Fe and W, while the Ni content includes contributions from both the Ni foam substrate and the Ni-based catalyst.

Table S2. EIS fitting parameters

Sample	**R_s** (Ω)	**R_{ct}** (Ω)	**Q** (CPE-T)	**n** (CPE-P)
NiFeWP(V_P)	0.588	0.964	3.41×10^{-6}	1.051
NiFeWP	0.486	2.147	2.06×10^{-6}	1.023
NiFeP(V_P)	0.496	0.934	6.45×10^{-6}	0.996
NiFeP	0.539	1.111	3.74×10^{-6}	1.036
NiWP(V_P)	0.474	1.079	4.69×10^{-6}	1.019
NiWP	0.574	1.996	4.34×10^{-6}	0.976

The EIS data were fitted using an equivalent circuit of R_s-(R_{ct} || CPE), where R_s represents the solution resistance, R_{ct} corresponds to the charge-transfer resistance, and CPE is the constant phase element.

Table S3. Comparison of OER electrocatalytic performance of NiFeWP(V_P) with recently reported phosphide catalysts and other types of catalysts in 1.0 M KOH.

Indices / **Materials**	**η_{10} (mA cm^{-2})**	**Tafel slope (mV dec^{-1})**	**Ref.**
NiFeWP(Vp)	**144**	**76**	**This wrok**
Ni_5P_4@FeP	205	43.93	S1
Mn-Co-Fe-P	192	43.75	S2
V_P-Ni_2P@NC	308	90.4	S3
$Fe_{0.1}Co_{0.4}W_{0.5}P$	250	48	S4
Fe-doped CoP	230	67	S5
$NiSe_2$/$FeSe_2$/CC	256	50	S6
NiFe-LDH/Ni_3S_2	202	45.1	S7
Ni_3FeN@PO_4^{3-}/NF	228	29.9	S8
$FeNiMoO_x$	235	56	S9
a/c-CoFe-LDH/Pt	253	85	S10
Ir_{25}-$Fe_{16}Ni_{100}P_{64}$	170	48	S11

Reference

[S1] Y. Li, Y. Wu, H. Hao, M. Yuan, Z. Lv, L. Xu, B. Wei, In situ unraveling surface reconstruction of Ni_5P_4@FeP nanosheet array for superior alkaline oxygen evolution reaction, *Appl. Catal. B Environ. Energy*, 2022, **305**, 121033. DOI: 10.1016/j.apcatb.2021.121033

[S2] F. Wang, Z. Pei, Z. Xu, T. Qin, X. Ouyang, D. Li, Y. Hou, X. Guo, Constructing Mn-Co-Fe ternary metal phosphides nanosheet arrays as bifunctional electrocatalysts for overall water splitting, *Adv. Sci.*, 2025, **12**, 2417521, DOI: 10.1002/advs.202417521

[S3] X. Guo, C. Lv, Y. Wang, T. Wang, X. Gan, L. Li, X. Lv, Nickel phosphonate MOF derived N-doped carbon-coated phosphorus-vacancies-rich Ni_2P particles as efficient bifunctional oxygen electrocatalyst, *Chem. Eur. J*, 2023, **29**, e202302182, DOI: 10.1002/chem.202302182

[S4] Y. Zhu, T. Chen, Z. Zhao, S. Zhang, B. Ding, D. Chen, G. Chen, Origin of enhanced performance on trimetallic phosphide electrodes for alkaline water oxidation, *ACS Appl. Energy Mater.*, 2025, **8**, 8543-8550. DOI: 10.1021/acsaem.5c01032

[S5] C. Tang, R. Zhang, W. Lu, L. He, X. Jiang, A.M. Asiri, X. Sun, Fe-doped CoP nanoarray: a monolithic multifunctional catalyst for highly efficient hydrogen generation. *Adv. Mater.*, 2017, **29**, 1602441, DOI: 10.1002/adma.201602441

[S6] S. Ni, H. Qu, Z. Xu, X. Zhu, H. Xing, L. Wang, J. Yu, H. Liu, C. Chen, L. Yang, Interfacial engineering of the $NiSe_2/FeSe_2$ p-p heterojunction for promoting oxygen evolution reaction and electrocatalytic urea oxidation, *Appl. Catal. B Environ. Energy*, 2021, **299**, 120638, DOI: 10.1016/j.apcatb.2021.120638

[S7] W. Wu, Y. Wang, S. Song, Z. Ge, C. Zhang, J. Huang, G. Xu, N. Wang, Y. Lu, Z. Deng, H. Duan, M. Liu, C. Tang, Built - in electric field in freestanding hydroxide/sulfide heterostructures for industrially relevant oxygen evolution. *Angew. Chem. Int. Ed.*, 2025, **137**, e202504972, DOI: 10.1002/anie.202504972

[S8] H. Hu, X. Wang, Z. Zhang, J. Liu, X. Yan, X. Wang, J. Wang, J.P. Attfield, M.

Yang, Engineered nickel–iron nitride electrocatalyst for industrial-scale seawater hydrogen production. *Adv. Mater.*, 2025, **37**, 2415421. DOI: 10.1002/adma.202415421

[S9] J. Ke, J. Zhang, L. Zhang, S. He, C. Zhong, L. Du, H. Song, X. Fang, Z. Zhang, Z. Cui, Role of High-Valence Metal Dissolution in Oxygen Evolution Kinetics of the Advanced $FeNiO_x$ Catalysts. *ACS Catal.*, 2024, **14**, 16363-16373. DOI: 10.1021/acscatal.4c04454

[S10] C. Gong, W. Li, X. Du, X. He, D. Wang, H. Chen, W. Fang, L. Zhao, Y. Chai, Manipulating spin polarization by in-situ reconstructed amorphous/crystalline CoFe-LDH for efficient electrocatalytic water splitting, *Nano Res.*, 2025. DOI: 10.26599/nr.2025.94907668

[S11] N. Yang, S. Tian, Y. Feng, Z. Hu, H. Liu, X. Tian, L. Xu, C. Hu, J. Yang, Introducing high-valence iridium single atoms into bimetal phosphides toward high-efficiency oxygen evolution and overall water splitting, *Small*, 2023, **19**, 2207253. DOI: 10.1002/smll.202207253